OUKA
Osaka University Knowledge Archive

Title	Modal Analysis of Guided Waves in a Bar with Arbitrary Cross-Section
Author(s)	Hayashi, Takahiro; Suyama, Mitsunobu; Abe, Tsukasa
Citation	Journal of Solid Mechanics and Materials Engineering. 2008, 2(5), p. 636-644
Version Type	AM
URL	https://hdl.handle.net/11094/84515
rights	© 2008 by The Japan Society of Mechanical Engineers.
Note	

Osaka University Knowledge Archive : OUKA

https://ir.library.osaka-u.ac.jp/

Osaka University

Journal of Template

Vol. 00, No. 0, 0000

Modal analysis of guided waves in a bar with arbitrary cross-section*

Takahiro Hayashi** Mitsunobu Suyama** and Tsukasa Abe***

**Nagoya Institute of Technology,
Gokiso Showa Nagoya, 466-8555, Japan
E-mail: hayashi@nitech.ac.jp
***JR East Technical center,
2-0 Nisshin-cho, Kita-ku Saitama, 331-8513, Japan

Abstract

Guided waves, i.e., ultrasonic wave packets propagating in the longitudinal direction, are a promising technique for rapid long-range nondestructive inspection of bar-like structures such as pipes and rails. Guided wave inspection requires determining guided wave velocities (dispersion curves) and wave structures. A computational technique is available to obtain the dispersion curves and wave structures for structures with complex cross-sections. This study develops a more accurate technique using the mirror relation of guided wave modes and an iteration method for solving the eigenproblem. Experimental studies of a JIS 6-kg rail verify that dispersion curves and wave structures can be obtained with sufficient accuracy for typical out-of-plain vibration modes. Wave structures were obtained by measuring waveforms at several points on the curved surface of the rail with a laser interferometer controlled by robot arms.

Key words: Ultrasonic nondestructive inspection, Guided waves, Dispersion curves, Rail, Curved surface scanning

1. Introduction

When a low-frequency ultrasonic wave below a few hundred kHz is input into pipes and rails, ultrasonic modes propagating in the longitudinal direction, called a guided wave, are observed. Guided waves exhibit long-range propagation of the order of ten to a hundred meters. It is expected that the long-range propagation in guided waves will enable fast inspection of large structures and remote inspection of unreachable parts [(1)–(3)].

In defect detection in pipes and rails with guided waves, the arrival time of defect echoes and guided wave velocities are used to determine the location of a defect, similar to ordinary ultrasonic inspection. The guided wave velocities can be analytically obtained for such simple structures as plates and pipes [(4), (5)]. The velocities can be graphed as curves with frequency versus phase velocity or group velocity, called dispersion curves. The dispersion curves describe the number of guided wave modes and dispersion in the frequency region. Wave structures in a cross-section can also be obtained analytically, enabling the most suitable guided wave mode to be selected, allowing the design of exciting and receiving transducers for guided wave inspection.

Thus, dispersion curves and wave structures are fundamental information for guided wave analysis. Although they cannot be obtained analytically for a bar with a complex cross-section, such as railway rails and H shape beams, guided waves are known to propagate long range in large structures[(6)] and are regarded as a promising technique for large structure inspection.

*Received XX Xxx, 200X (No. XX-XXXX)
[DOI: 00.0000/ABCDE.2006.000000]

The authors have developed a technique for deriving dispersion curves and wave structures for a bar with an arbitrary cross-section using a special finite element method called the semi-analytical finite element method (SAFEM) [7]–[9]. In SAFEM, the cross-section is divided two-dimensionally and the longitudinal direction is expressed by an orthogonal function $\exp(ikz)$. Then, as a necessary condition for the governing equation to obtain solutions, an eigenvalue problem with respect to wave number k is solved. The eigenvalues and eigenvectors obtained from the eigensystem denote the wave numbers and wave structures of the eigenmodes. Dispersion curves calculated by SAFEM have been experimentally confirmed in reference (8) with a two-dimensional Fourier transform technique.

However, our previously determined eigenvalues and eigenvectors were limited to about 100 nodes using common personal computers due to the large computational time and memory required [8]. Therefore, our previous solutions exhibited problems, such as eigenvalues having slightly different values and certain eigenvalues not appearing in some subdivisions. Theoretical dispersion curves obtained by calculation were compared with experimental dispersion curves with a two-dimensional Fourier transform technique, but the theoretical wave structures could not be confirmed in our previous work. In order to obtain wave structures experimentally, a large number of waveforms should be measured at sufficiently close discrete points, which is difficult for curved surfaces such as railway rails.

This study describes a highly accurate computational technique for dispersion curves and wave structures with small cross-sectional subdivisions using the symmetric characteristic of guided wave modes and a projection method for the large eigenvalue problem called the implicit restarted Arnordi method. Guided waves are also measured at a large number of points on a curved surface of a rail to obtain wave structures experimentally using a laser Doppler interferometer equipped with a robot arm.

2. Derivation of dispersion curves and wave structures by the semi-analytical finite element method

2.1 Brief description of the semi-analytical finite element method

In the ordinary finite element method, the calculation region is divided into small elements and the wave field in the region is expressed by the displacements at the vertexes of the elements (nodes) and the interpolation function (shape function). Generally, a governing equation is obtained by minimizing the potential energy in the whole region when the displacements at the nodes are taken to be unknown parameters:

$$\mathbf{F} = \mathbf{K}\mathbf{U} - \omega^2\mathbf{M}\mathbf{U}, \tag{1}$$

where $\mathbf{F}$ and $\mathbf{U}$ are the nodal force and displacement vectors, respectively, and $\mathbf{K}$ and $\mathbf{M}$ are the kinetic and mass matrices, respectively. This governing equation can be solved for a certain angular frequency ω. In contrast, in SAFEM, only the cross-section is divided into small elements, and the longitudinal (z) direction is expressed by $\exp(i\xi z)$. Then, the wave field with respect to the wave number ξ is expressed. The following eigenvalue problem is obtained by minimizing the potential energy in the whole region expressed by the nodal displacements:

$$\mathbf{F} = \left(\mathbf{K}_1 + i\xi\mathbf{K}_2 + \xi^2\mathbf{K}_3 - \omega^2\mathbf{M}\right)\mathbf{U}, \tag{2}$$

where $\mathbf{K}_1$, $\mathbf{K}_2$, $\mathbf{K}_3$ and $\mathbf{M}$ are $M\times M$ real symmetric matrices, with M the degree of freedom. In three-dimensional cases, there are three times the number of nodes. This eigenvalue problem can be transformed into the following generalized eigenvalue problem using $2M \times 2M$ matrices $\mathbf{A}$ and $\mathbf{B}$, following references (10) and (11):

$$\left(\mathbf{A} - \xi\mathbf{B}\right)\mathbf{Q} = \mathbf{p} \tag{3}$$

$$\left.\begin{aligned}\mathbf{A}&=\begin{bmatrix}\mathbf{0} & \mathbf{K}_1-\omega^2\mathbf{M}\\ \mathbf{K}_1-\omega^2\mathbf{M} & i\mathbf{K}_2\end{bmatrix},\\ \mathbf{B}&=\begin{bmatrix}\mathbf{K}_1-\omega^2\mathbf{M} & \mathbf{0}\\ \mathbf{0} & -\mathbf{K}_3\end{bmatrix},\\ \mathbf{Q}&=\begin{bmatrix}\mathbf{U}\\ \xi\mathbf{U}\end{bmatrix},\quad \mathbf{p}=\begin{bmatrix}\mathbf{0}\\ \mathbf{F}\end{bmatrix}.\end{aligned}\right\} \tag{4}$$

In order to obtain a solution for eq. (3), ξ should be a set of 2*M* eigenvalues for the following eigenvalue problem:

$$(\mathbf{A}-\xi\mathbf{B})\mathbf{Q}=\mathbf{0} \tag{5}$$

The 2*M* eigenvalues ξ_m (m = 1…2*M*) represent the wave numbers of the eigenmodes. Assuming that the nodal displacement vector for the *m*th eigenmode is $\mathbf{U}_m$, the eigenvector corresponding to the eigenvalue ξ_m is given by

$$\mathbf{\Phi}_m=\begin{bmatrix}\mathbf{U}_m\\ \xi_m\mathbf{U}_m\end{bmatrix}. \tag{6}$$

The 2*M* eigenvalues include *M* wave numbers for forward waves and *M* for backward waves [7]–[9]. It should be noted that, in this case, the nodal force vector shown in eq. (5) is set to zero. Namely, the solution obtained here is for the case of zero external loading. This corresponds to the fact that dispersion curves are obtained for regions without fastenings and supports in the experiments in Section 3 in this paper.

2.2 Reduction of the order of the eigenvalue problem using the symmetry of forward and backward waves

All eigenvalues and eigenvectors obtained from eq. (5) consist of *M* pairs of wave numbers for forward and backward waves. A pair of forward and backward waves is symmetric in having the same wave number with different signs, and the same wave structure with different signs only in the *z*-direction. That is, the eigenvalue for a backwards wave can be written -ξ, corresponding to the eigenvalue of ξ for the forward wave. The eigenvectors of the backward and forward waves can be written

$$\mathbf{U}^{-}=\begin{bmatrix}\mathbf{U}_{xy}\\ -\mathbf{U}_z\end{bmatrix}, \tag{7}$$

$$\mathbf{U}^{+}=\begin{bmatrix}\mathbf{U}_{xy}\\ \mathbf{U}_z\end{bmatrix}, \tag{8}$$

respectively, where $\mathbf{U}_z$ denotes a vector with *M*/3 displacement components in the *z* direction and $\mathbf{U}_{xy}$ denotes the other 2*M*/3 components.

We now consider the following equation:

$$(\mathbf{K}_1-\omega^2\mathbf{M}+i\xi\mathbf{K}_2+\xi^2\mathbf{K}_3)\mathbf{U}=0, \tag{9}$$

which is obtained by setting the nodal force vector to zero in eq. (2). For the forward wave, separated only in the z direction we have

$$\left[(\mathbf{K}_{11}\quad\mathbf{K}_{12})+i\xi(\mathbf{K}_{21}\quad\mathbf{K}_{22})+\xi^2(\mathbf{K}_{31}\quad\mathbf{K}_{32})\right]\begin{pmatrix}\mathbf{U}_{xy}\\ \mathbf{U}_z\end{pmatrix}=0, \tag{10}$$

$$\mathbf{K}_1-\omega^2\mathbf{M}=(\mathbf{K}_{11}\quad\mathbf{K}_{12}),\ \mathbf{K}_2=(\mathbf{K}_{21}\quad\mathbf{K}_{22}),\mathbf{K}_3=(\mathbf{K}_{31}\quad\mathbf{K}_{32}). \tag{11}$$

The following equation applies for backward waves:

$$\left[(\mathbf{K}_{11}\quad\mathbf{K}_{12})-i\xi(\mathbf{K}_{21}\quad\mathbf{K}_{22})+\xi^2(\mathbf{K}_{31}\quad\mathbf{K}_{32})\right]\begin{pmatrix}\mathbf{U}_{xy}\\ -\mathbf{U}_z\end{pmatrix}=0 \tag{12}$$

The following equation is obtained from [(eq.(10)+eq.(12)) × ξ + (eq.(10) - eq.(12))]/2:

$$\left[(\mathbf{K}_{11}+i\mathbf{K}_{21}\quad\mathbf{K}_{12})-\xi^2(-\mathbf{K}_{31}\quad-i\mathbf{K}_{22}-\mathbf{K}_{32})\right]\begin{pmatrix}\xi\mathbf{U}_{xy}\\ \mathbf{U}_z\end{pmatrix}=0 \tag{13}$$

This equation can be transformed into an eigenvalue problem consisting of *M* × *M* matrices

$\mathbf{H}_1$ and $\mathbf{H}_2$:

$$(\mathbf{H}_1 - \eta\mathbf{H}_2)\mathbf{V} = 0\,, \tag{14}$$

$$\left.\begin{aligned} &\mathbf{H}_1 = \begin{pmatrix}\mathbf{K}_{11} + i\mathbf{K}_{21} & \mathbf{K}_{12}\end{pmatrix},\quad \mathbf{H}_2 = \begin{pmatrix}-\mathbf{K}_{31} & -i\mathbf{K}_{22} - \mathbf{K}_{32}\end{pmatrix}, \\ &\mathbf{V} = \begin{pmatrix}\xi\mathbf{U}_{xy} \\ \mathbf{U}_z\end{pmatrix}, \qquad \eta = \xi^2\,. \end{aligned}\right\} \tag{15}$$

For the M eigenvalues obtained from eq. (14), η_m (m=1,2,…,M), taking $\xi_m = \pm\sqrt{\eta_m}$ gives the wave numbers for the forward and backward waves. The eigenvectors obtained give

$$\mathbf{V}_m = \begin{pmatrix}\xi_m\mathbf{U}_{xy\,m} \\ \mathbf{U}_{z\,m}\end{pmatrix}. \tag{16}$$

Hence, dividing the components in the x and y directions by ξ_m gives the cross-sectional displacement vector for the mth mode as

$$\mathbf{U}_m = \begin{pmatrix}\mathbf{U}_{xy\,m} \\ \mathbf{U}_{z\,m}\end{pmatrix}. \tag{17}$$

Using the above process, the size of the matrices in the eigenvalue problem decreases by half and the number of nodes can be double that of other previous techniques.

2.3 Calculating eigenvalues for lower order modes using the projection method for the large eigenvalue problem

Eigenvalue problems with complex generalized matrices can be solved using programs such as the GVCCG subroutine for IMSL. GVCCG calculates all the eigenvalues and eigenvectors, but it is not suitable for large eigenvalue problems due to the large computational time required, approximately proportional to the cube of the matrix size.

Therefore, in this study we use the implicit restarted Arnordi method, a projection method for large eigenvalue problems, to calculate dispersion curves for a rail structure with high accuracy. The Arnordi method can solve a very large eigenvalue problem $\mathbf{A}\boldsymbol{x}=\lambda\,\boldsymbol{x}$ because the large eigenvalue problem is approximated by a smaller eigenvalue problem by the projection of subspaces. In this method, not all the eigenvalues and eigenvectors are obtained, however, since dispersion curves for guided wave inspection need only propagating modes with real wave numbers, this method gives sufficiently accurate solutions. In this paper, we use a Fortran subroutine for the Arnordi method called ARPACK[14].

3. Dispersion curves for a 6-kg rail

As an example, dispersion curves for a JIS 6-kg rail are obtained here. Fig. 1 shows cross-sectional meshes with the maximum number of nodes (a) for the IMSL subroutine GVCCV from our previous work, with 107 nodes, and (b) for the ARPACK subroutine, with 718 nodes, using a common PC. In our previous work using GVCCV, we obtained very course cross-sectional elements (Fig. 1 (a)), for which the calculations were likely to be less accurate. Fig. 2 shows dispersion curves obtained for these cross-sectional elements, as well as for 360 nodes using the ARPACK (red square). In the low-frequency region below 20 kHz, the solutions are almost the same. However, the differences between them increase as the frequency increases. The 360-node data is closer to the 718-node data than the 107-node data, showing a shift to higher accuracy as the number of nodes increases. As observed from several further results for different node numbers, the calculation results are sufficiently accurate in the case of Fig. 1 (b).

The cross-sectional subdivisions shown in Fig.1 were set to be symmetric with respect to the center vertical line. If the subdivisions are not symmetric, even for a symmetric cross-section, a symmetric mode shape may sometimes distort, resulting in a small error in

the solutions of the dispersion curves and wave structures [12].

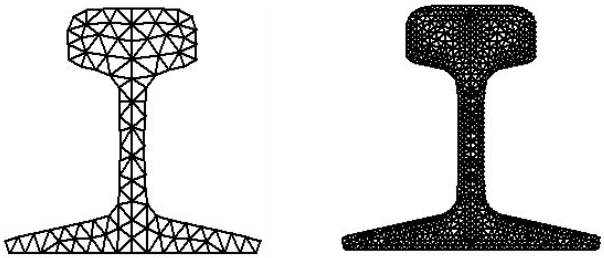

(a) (b)

Fig. 1 Cross sectional division for calculations of dispersion curves with (a) IMSL GVCCV (107 nodes) and (b) ARPACK (718 nodes).

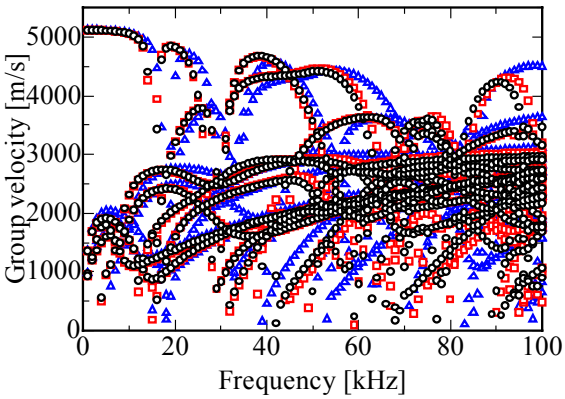

Fig. 2 Group velocity dispersion curves for JIS 6-kg rails derived from (a) (107 nodes, blue triangle) and (b) (718 nodes, black circle) in Fig.1 and a 360-node model (red square).

4. Experimental verification of wave structures

Fig. 3 shows dispersion curves for a JIS 6-kg rail obtained by the cross-sectional division of Fig. 1 (b) below 60 kHz. At 37 kHz, two modes with large group velocities can be seen, indicated by (A) and (B). These are longitudinal vibrating modes observed experimentally in our previous work [14]. We found that the mode with the largest group velocity (A) vibrates with the same phase at the upper and lower areas of the cross-section. Mode (B) exhibits the opposite vibration at the upper and lower areas. In this section, measured wave structures for the other modes with lower group velocities (a)–(e) at 37 kHz are presented.

Fig. 4 shows the wave structures (a)–(e) corresponding to the eigenvectors obtained by the SAFE calculation described in the previous section. Displacements normal to the cross-section are not shown in these figures because they were small compared to the in-plane displacements. The red and black lines denote the original position of the structure and the position of the deformed structure after a quarter period, respectively, which correspond to the imaginary and real parts of the eigenvectors described by eq. (17).

Inspecting these wave structures reveals that (a) and (b) are modes vibrating horizontally at the web, (c) is a mode vibrating vertically at the head, and (d) and (e) are modes vibrating flexurally at the bottom.

In order to verify these calculated wave structures, guided waves were measured at several points on the surface of a rail with a laser Doppler vibrometer equipped with a robot arm. Fig. 5 shows the experimental set-up. A function generator generated a four-cycle burst wave at a center frequency of 37 kHz. A voltage of about 150Vp-p was applied to an

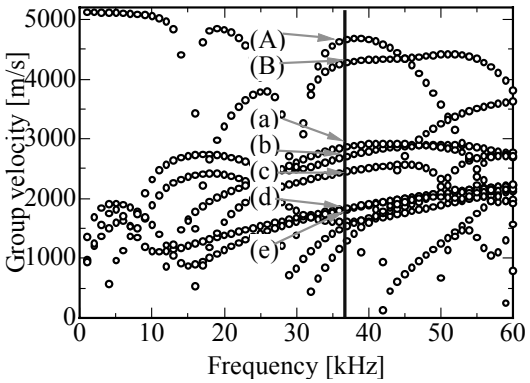

Fig. 3 Group velocity dispersion curves for JIS 6-kg rails (718 nodes).
The vertical line denotes 37 kHz. (A) and (B) are modes with longitudinal vibrations.
The wave structures for (a)–(e) are given in Fig. 4.

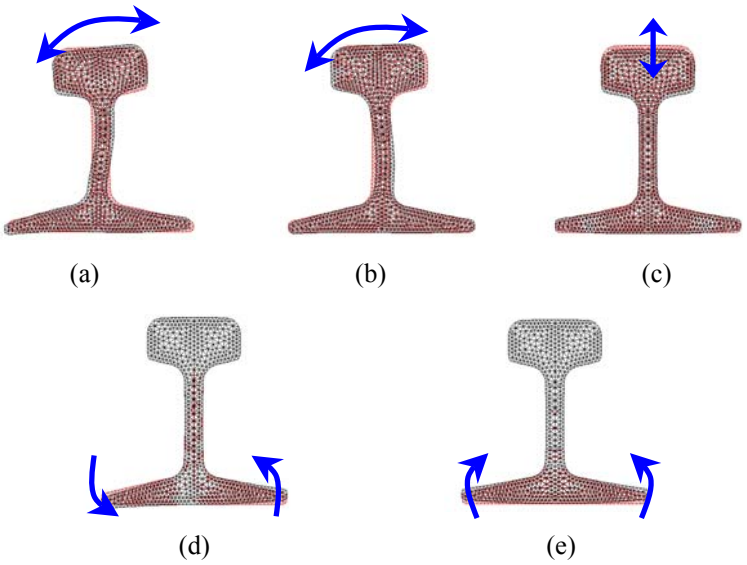

Fig. 4 Wave structures for several guided wave modes in a JIS 6-kg rail at 37 kHz.
The structures (a)–(e) correspond to dispersion curves (a)–(e) in Fig. 3. The red and black lines denote the original position of the structure and the position of the deformed structure after a quarter period, respectively.

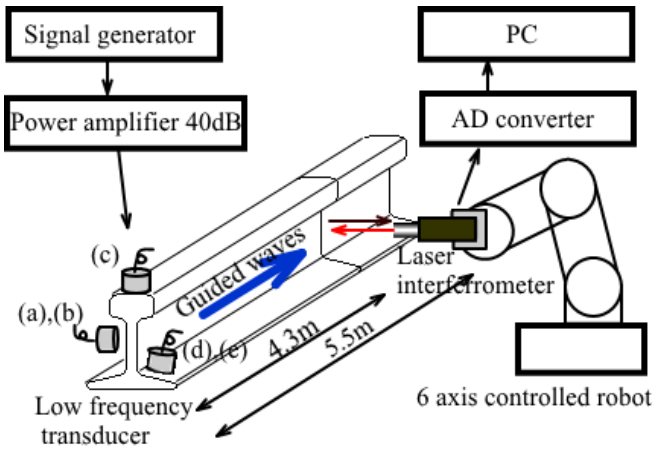

Fig. 5 Experimental set-up for guided wave measurement.

excitation contact transducer.

The low frequency transducer was set on the web for (a) and (b), on the upper surface of the head for (c) and on the upper surface of the bottom for (d) and (e) so as to excite each mode effectively. The dimension of a JIS 6-kg rail is 50.8 mm in height and 50.8 mm in width, which is about 1/3 of the cross-section of general railway rails. The length of the rail was 5.5 m. Guided waves were excited at one end of the rail and received 4.3 m from that end. The laser Doppler vibrometer (Ono Sokki, LV-1720) was used as a receiver and reflection tapes (Ono Sokki, LV-0012) were attached at the measurement areas to receive waves stably even with auto scanning by the robot arm. The sensing part of the laser Doppler vibrometer was equipped with a robot arm (Mitsubishi Electric, RV-6S) and the laser beam was set to be incident normal to the rail surface. At the receiving points at 4.3 m, reflected waves from the far end 5.5 m away from the excitation transducer did not interfere with the direct incident waves of the modes (a)–(e). However, the reflected waves from the end close to the excitation transducer did interfere with the direct incident waves, but since the transducer was located very close to the end, the direct incident and reflected waves were superposed perfectly. Other reflected waves, such as those from supported points, were not seen in the detected signals. Therefore, reflected waves from either end did not affect the experimental wave structures, as shown later. Fig. 6 shows the scanning regions on the rail. Due to the limited motion space of the robot arm, the scanning areas were set to encompass only the right half of the rail, areas A–E. Vibration normal to the surface was detected at each region in 1-mm increments. The positioning accuracy of the robot arm was ±0.02 mm, which was sufficiently accurate to detect guided waves in this frequency range. In the regions A, B, C, D and E, there were 12, 7, 22, 17 and 26 measurement points, respectively, which were sufficient to describe the wave structures shown in Fig. 4.

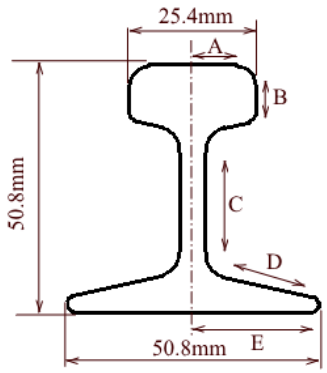

Fig. 6 Cross-section of a JIS 6-kg rail and scanning regions.

Fig. 7 shows the waveforms measured at 12 points in the region A when the excitation transducer was put on the web to verify the modes (a) and (b) in Figs. 3 and 4. The horizontal axis denotes the propagating time. Since the arrival time for these modes can be estimated at about 1520 μs and 1590 μs, respectively, from the group velocities of (a) and (b) in Fig. 3, the first wave packet seen in the time range from 1500 μs to 2000 μs contains both modes (a) and (b). Using the signals detected in the region A–E, wave structures are constructed in Fig. 8, where the signals are expressed as out-of-plane displacement at the measured points. Figs. 8 (a) and (b) show the distortion of the cross-section at 1585 μs and 1720 μs for web excitation, which could correspond to the modes (a) and (b) in Figs. 3 and 4. Fig. 8 (a) agrees well with Fig. 4 (a), where region A inclines upward and region C (web) has a node, i.e. a symmetric point of deformation, at the center. Fig. 8 (b) also agrees well with Fig. 4 (b), where region C vibrates with nodes at the upper and lower edges and with an anti-node at the center. Similarly, Fig. 8 (c), showing the cross-sectional wave structure

obtained when the excitation transducer was put on the railhead, agrees well with Fig. 4 (c), showing the calculated cross-sectional wave structure. Fig. 8 (d) shows the distortion when an ultrasonic vibration is applied on the rail bottom. This wave structure appears to show a mixed mode of (d) and (e), because the group velocities of (d) and (e) are almost identical in the dispersion curves of Figs. 3(d) and (e). Since both these modes vibrate largely at the bottom of the rail, Fig. 8(d) expresses them very well.

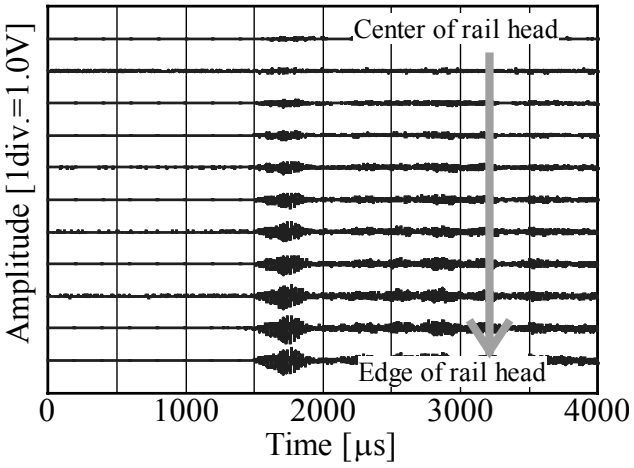

Fig. 7 Waveforms detected at region A for normal incidence on the rail web.

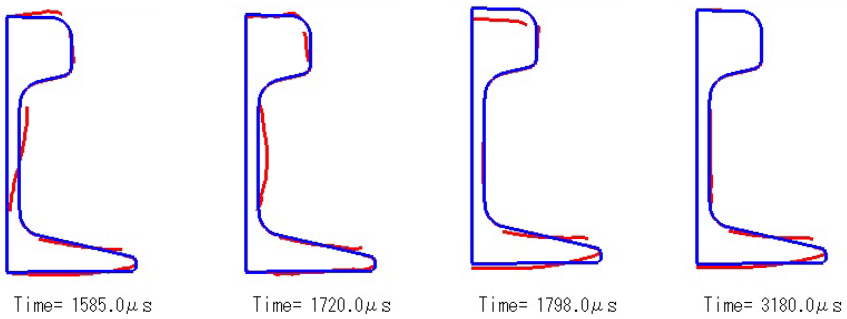

Fig. 8 Displacement detected at several points on the rail surface with a laser interferometer. (a)–(c) show the modes (a)–(c) from Fig. 4 and (d) shows a mixed mode of (d) and (e) from Fig. 4. The blue and red lines denote the original position of the structure and the position obtained from the measured waveforms

6. Conclusions

As method to derive guided wave dispersion curves and wave structures for a bar with an arbitrary cross-section with high accuracy, the symmetry of guided wave modes and the Arnordi projection method for large eigenvalue problems were applied to the semi-analytical finite element method. The computational technique was verified through a comparison between the wave structures obtained by calculation and experiment for a JIS 6-kg rail. The experimental wave structures were obtained by measuring wave forms at several points on the surface of a rail using a laser Doppler vibrometer equipped with a robot arm with sufficient positioning accuracy.

This scanning technique can be applied to any curved structures by changing the scanning program.

References

(1) Nishino, H., Journal of the Japanese Society of Non-destructive Testing, Vol. 52, No. 12 (2003), pp. 654–661.
(2) Cawley, P. et al., Materials Evaluation, Vol. 61, No. 1 (2003), pp. 66–74.
(3) Hayashi, T., Journal of the Japanese Society of Non-destructive Testing, Vol. 54, No. 11 (2004), pp. 590–594.
(4) Gazis, D. C., Journal of the Acoustical Society of America. Vol. 31, No. 5 (1959), pp. 568–578.
(5) Nishino, H. et al., Japanese Journal of Applied Physics, Vol. 40, No. 1A (2001), pp. 364–370.
(6) Rose, J. L. et al., Insight, Vol. 44, No. 6 (2002), pp. 353–358.
(7) Hayashi, T., Japanese Society of Non-destructive Testing, Vol. 52, No. 12 (2003), pp. 662–666.
(8) Hayashi ,T. et al., Ultrasonics, Vol. 41, No. 3 (2003), pp. 175–183.
(9) Hayashi ,T. et al., Ultrasonics, Vol. 44, No. 1 (2006), pp. 17–24.
(10) Zienkiewicz, O. C., The Finite Element Method, Third Edition (1977), McGraw-Hill.
(11) Dong, S. B., International Journal for Numerical Methods in Engineering, Vol.11 (1977), pp. 247–267.
(12) Editorial Committee of Modal Analysis Handbook, Modal Analysis Handbook (2000) Corona Publishing.
(13) Arnordi, W. E., Quart. J., Applied Mathematics, Vol. 9 (1951), pp. 17–29.
(14) Sorensen, D. C., SIAM Journal on Matrix Analysis and Applications, Vol. 13, No. 1 (1992), pp. 357–385.
(15) Li, S. et al., Proceedings of JSNDI Spring Conference 2005, pp. 145–148.